

An irreversible growth model for virus capsid assembly

Stephen D. Hicks* and C. L. Henley†

Department of Physics, Cornell University, Ithaca, New York 14853

We model the spontaneous assembly of a capsid (a virus's closed outer shell) from many copies of identical units, using entirely irreversible steps and only information local to the growing edge. Our model is formulated in terms of (i) an elastic Hamiltonian with stretching and bending stiffness and a spontaneous curvature, and (ii) a set of rate constants for addition of new units or bonds. An ensemble of highly irregular capsids is generated, unlike the well-known icosahedrally symmetric viruses, but (we argue) plausible as a way to model the irregular capsids of retroviruses such as HIV. We found that (i) the probability of successful capsid completion decays exponentially with capsid size; (ii) capsid size depends strongly on spontaneous curvature and weakly on the ratio of bending and stretching elastic stiffnesses of the shell; (iii) the degree of localization of Gaussian curvature (a measure of facetedness) depends heavily on the ratio of elastic stiffnesses.

I. INTRODUCTION

In recent years the question of spontaneous assembly has arisen in many apparently disconnected fields, including nanofabrication [1, 2], robotics and microelectronics [3, 4], and particularly biology [5, 6]. Among biological systems that assemble themselves are protein molecules, microtubules, and actin. For many biological structures, assembly requires energy in the form of ATP hydrolysis [7–9], but for numerous others it runs spontaneously: in particular that of lipid bilayers [10, 11] and of virus capsids [12, 13], the subject of this paper.

A. Quasiequivalence

The capsid of a virus is the shell of proteins surrounding and protecting the viral genome (nucleic acid). Capsids are observed in a wide range of sizes, ranging into the thousands of proteins; most known capsids have icosahedral or cylindrical point group symmetry [14, 15]. A typical virus uses only one, or a few, kinds of protein in its capsid; consequently noted, typical capsids are necessarily built from copies of the same units in positions that are *not* equivalent by any global symmetry [16]. However, Caspar and Klug [16] identified an elegant approximate symmetry which they called *quasiequivalence*. The key idea is that locally, every bit of the capsid is a patch of triangular lattice; in an infinite triangular lattice, all the units *would* be symmetry equivalent. They argued that typical proteins could accommodate a variation of $\pm 5^\circ$ in bond angles [17], while maintaining the same microscopic bonding between proteins. This allows representation of any capsid as a network of approximately equilateral triangles, with a constraint (due to the angle limitation) that the number of triangles around every vertex must always be either five or six.

The points of local five-fold symmetry may be identified with the topological defects called *disclinations* (to be defined in Sec. II A), and any closed shell must contain exactly twelve of them. In any icosahedral capsid, the disclinations form the vertices of a large icosahedron, the edges of which have length \sqrt{T} in lattice units, where the triangulation number $T = 1, 3, 4, 7, \dots$ is one of a sequence of discrete allowed integers [16], so there are $60T$ small triangles.

We emphasize that the rules of quasiequivalence do not force any global symmetry, nor do they fix the size of the completed capsid. Thus it is surprising that many viruses reliably assemble large symmetric capsids. The challenge to theory is to explain both the size and shape selection, or at the least to explain why a closed shell is formed, when tubes or sheets would be equally consistent with the local bonding. It would not be surprising if models predict different capsids depending on parameters (which might experimentally correspond to pH, salt content, catalysts, protein concentrations, or mutations in the capsid protein). Such polymorphic behavior is very fruitful to study in quasiequivalent models: it effectively explores more of the various local geometries in which the proteins can bind and thus can allow more parameters to be determined, in principle. This paper develops a model of irreversible (non-equilibrium) assembly of quasiequivalent units which produces a highly polymorphic ensemble of capsids, which we argue below may model the growth of retrovirus capsids.

B. Recent Models

The most successful recent capsid models consistent with quasiequivalence are *equilibrium* theories: a microscopically motivated phenomenological Hamiltonian is shown to be optimized by certain shapes, and it is assumed that this free energy minimum is found during the actual assembly process. Thus Bruinsma, *et al.* [13, 18] modeled pentamers and hexamers as different-sized discs packed on a sphere, with an effective Hamiltonian favoring dense packing, a bending stiffness with

*Electronic address: sdh33@cornell.edu

†Electronic address: clh@ccmr.cornell.edu

spontaneous curvature, and a switching cost to make pentamers (rather than hexamers) of the proteins. When this switching cost is small, icosahedral viruses were selected over nonicosahedral shapes [18]. Additionally they demonstrated polymorphism, similar to phenomena seen in Cowpea Chlorotic Mottle Virus (CCMV), by showing a phase transition between tubes, $T = 3$, and $T = 1$ capsids as the model parameters varied. Another family of models, introduced by Nelson, focuses on the external shape of large capsids, using continuum elastic theory: the shape evolves from practically spherical to sharply faceted as the size increases or the bending rigidity decreases.

Alternate theories to quasiequivalence have also been developed, still in terms of an equilibrium picture. Most notable is the “local rules” theory [19–21] which posits several “flavors” of unit, with *inequivalent* edges, and rules for the joining of different kinds of edges so the units fit together like puzzle pieces and there is a single unique structure that obeys all the matching rules. It is generally necessary to assume that the same capsid protein molecule has different conformation species, each of which has entirely different specific binding. It appears implausible that so many different functions could be built into one molecule, or that evolution could have discovered this solution, if it is the only way to engineer a large capsid. We therefore prefer a theory without such matching rules.

Another class of theory focuses on the *process* of assembly, which one expects is far from equilibrium. Zlotnick [22, 23] has focused on the kinetics of capsid growth. Using a basic unit of $5T$ proteins, so that the complete capsid is a dodecahedron of 12 units, and a free energy based on the number of adhered edges, he considers the species of the most stable incomplete capsid of any size and constructs rate equations relating the concentrations of each species. This leads to the phenomenon of the kinetic trap: if the initial concentration of monomers is too large, they aggregate quickly into larger structures, slowing the later stages of growth since the required monomers are depleted.

C. Retroviruses

Retroviruses are RNA viruses which all contain a characteristic enzyme, reverse transcriptase, allowing the RNA to be transcribed to DNA inside the cell nucleus. Upon infection, the virus produces many copies of several proteins, in particular the structural polyprotein Gag. Approximately 5000 copies of Gag aggregate at the cell membrane before budding out of the cell as an immature virus particle. A maturation step then takes place in which a protease cleaves Gag into its constituent proteins: matrix (MA), capsid (CA), and nucleocapsid (NC). After cleavage, the MA remain bound to the lipid membrane and the NC remain bound to the RNA. Roughly 30% of the CA proteins then reassemble into the mature cap-

sid [24].

The previous sections have been limited to icosahedral viruses. While there is some polymorphism in icosahedral viruses, usually changing T numbers under different conditions, the capsids remain regular and symmetric. Retroviral capsids, on the other hand, have been observed to be very irregular. Ganser et al. [25] pointed out that the cones formed by mature human immunodeficiency virus (HIV) cores must have quantized angles and measured this with early three-dimensional reconstructions. Later studies have measured these angles and other data using more accurate tomography [26–28]. In addition to the irregular structure, polymorphism is also observed in the switching between tubes and spheres under different conditions [29]. Another retrovirus, Rous Sarcoma Virus (RSV), has cores that are observed to be roughly spherical, but with a wide distribution in the degree of asphericity [30].

There is significant variation in size and shape of HIV mature capsids, but they are commonly cones. Following the quasiequivalence paradigm, these are described geometrically by locally triangular lattices like carbon fullerene cones [28, 31]. There is no established explanation of the cone’s shape or size. Briggs et al. [26] suggest that the small end of the cone forms first, possibly from a sort of template, and that the large end forms when the growing capsid runs into the membrane. Benjamin et al. [27] instead suggest that the large end is nucleated first. Nguyen et al. [32] developed an equilibrium theory combining the ideas of Refs. [13] and [33], adding fullerene cones [31] to consideration. Assuming a fixed size, they generate a family of configurations of maximum symmetry, and find a phase transition between cones, tubes, and spheres as a function of the elastic parameters. A weakness of their model, however, is that cones are stable in a relatively small portion of parameter space, and their appearance at all depends critically on the fixed-size assumption, which is not physical. In HIV maturation, only a third of the capsid proteins assemble into the mature conical capsid, leaving the rest in solution within the virus’ lipid envelope [24]. Thus, we should expect the capsid size to vary freely.

D. Outline

In the following pages we present our model of capsid assembly, discussing our choice of energy and transitions which govern growth of a capsid from a single unit to a complete closed shell, by alternately minimizing the energy and choosing a transition to a larger capsid.

We discuss common failure modes arising in this model and the choices of parameters leading to them. In particular, we look at a failure which occurs at the end of growth in which a small hole cannot be completed, and a failure which occurs in the middle stages of growth.

We then consider a number of ways to measure growing and complete capsids, largely motivated by experimen-

tal measurements. We present in particular the effect of the spontaneous curvature parameter on the size of the grown capsids. We discuss ranges of parameters resulting in successful growth or in different failures. Lastly, we define measurements based on Gaussian curvature which are now experimentally possible due to advances in tomography.

Finally, we summarize our results and discuss the advantages and disadvantages of our model, and possible future directions.

II. IRREVERSIBLE GROWTH MODEL

We now introduce a model to describe quasiequivalent capsid assembly in a far from equilibrium picture. Consider a single growing capsid and a number of units in solution. We picture the units slowly accreting onto the growing capsid until the finished product is formed.

Our choice is to represent this by adopting the simplest possible model that can represent a growing capsid and be simulated efficiently: this precludes representing each protein as a rigid body moving in space. Instead, a capsid (growing or completed) is represented by a triangular network (Sec. II A), with an elastic energy governing the bond lengths and angles (Sec. II B). We do not explicitly represent the units in solution, instead formulating a set of first-order rate equations for addition of a unit to the capsid or for other discrete changes in the network geometry (Sec. II C).

Other physical or mathematical models have been abstracted to a similar degree [13, 18, 33], following a standard philosophy of statistical mechanics. Some capacity to adapt the model to (say) a specific virus species is lost, but the simplicity makes it conceivable to grasp the physical meaning of each parameter, and feasible to explore all dimensions of the parameter space by simulations. Typically, only particular combinations of the microscopic parameters matter, and a properly formulated toy model adopts those combinations. It can happen that fairly different microscopic systems may, through such elimination of unimportant parameters, all map to the same simple model; in that case, the model offers a possibility of unifying the description of all these systems.

A. Configuration degrees of freedom

Our formulation depends on *two* complementary kinds of degree of freedom, a discrete kind we call “topological” and a continuous kind called “positional”. The former consists of a bond network built from triangles, with vertices either connected by a bond or not; the latter consists of the actual coordinates of the vertices in space. Since prior work emphasized equilibrium, we took the opposite limit by allowing no change in any bond, once formed. One consequence is that our discrete “topological” variables are more fundamental than the positional

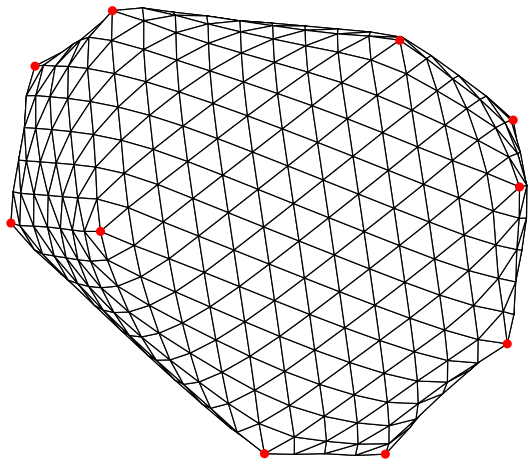


FIG. 1: Example of a closed final capsid resulting from our growth simulation, with $\ell_f = .12r_0$, $\theta_0 = 16^\circ$, $\Gamma_{I,J} = 50$, and $\sigma = 12.7^\circ$. These parameters are explained in Secs. II B-II C. The disclinations are marked by circles on the vertices.

ones: given a network of bonds, the angles and bond lengths will relax to a constrained minimum (or fluctuate thermally around it) as defined by a Hamiltonian, defined in Sec. II B. In our growth model, these positional variables feed back into the discrete ones by controlling the relative rates of alternative changes in the network as units are accreted. (In principle one could envisage a further abstraction in which the positional variables got eliminated and the rates were expressed directly in terms of the bond topology, but we did not attempt that.)

The models discussed above in Sec. I B all have basically just a single type of degree of freedom – the first, the second, or something intermediate. Lidmar et al. [33] assume a predetermined graph topology, so only the vertices’ positions are nontrivial. On the other hand, Endres et al. [34] discard(s) position information and only considers the (discrete) connectivity. Bruinsma et al. [13] continuously vary the positions of the discs, and determine which discs neighbor one another secondarily.

It may be questioned why we have chosen triangles as the fundamental building blocks. In a model more faithful to a particular virus species, one would want to add the multimer which is accreted in nature. Viruses assembling from dimers [35, 36], trimers [37], and pentamers/hexamers [38], have been seen experimentally, depending on the virus species. Several groups have done molecular dynamics simulations using solutions of monomers [19, 39] and kinetic simulations with pentamers [22], dimers [40], or trimers [41]. Because of its simplicity, and the work done on tethered surfaces by Nelson and coworkers [33, 42], we will focus on a trimer-based model for this initial work, an example of which can be seen in FIG. 1.

Our use of triangle units, rather than e.g. trapezoids (to represent monomers [39]) or hexamers/pentamers (as in Refs. [13] and [18]) is also influenced by the notion of “universality” in physics, whereby the functional form of

elastic theory, or the critical exponents of a phase transition, are independent of the particular lattice used at the microscopic scale. In any of the alternative representations, one can still define a triangular, locally sixfold lattice with rare locally 5-fold points in it. Much experience in statistical mechanics suggests that, at “coarse-grained” length scales (those large compared to the lattice spacing), the behavior stops depending on the details. However, two related caveats must be expressed, that (i) possibly a detail of the microscopic model forces a certain parameter of the coarse-grained model to be strictly zero, thereby changing the qualitative behavior (“universality class”); (ii) it may be that a parameter regime easy to achieve in one of the alternative versions of the model, will require a complicated fine-tuning of parameters in another version.

Caspar and Klug [16] noted that only pentamers and hexamers have small enough deformations to be allowed in quasiequivalence, and thus any quasiequivalent capsid must have exactly twelve pentamers. Quasiequivalence is based on a flat triangular lattice, so that a pentamer is a *disclination*, a topological defect of the triangular lattice. That means it can be characterized by effects at an arbitrary distance; namely, if we parallel transport a vector around a loop that vector ends up rotated by $(\pi/3)N_{\text{disc}}$ from its starting orientation, where N_{disc} is the number of 5-fold disclinations enclosed by the loop. (This is called a “disclination charge” by analogy to how the electric charge enclosed by a surface is determined by an integral of the electric field over that surface, according to Gauss’s law.) That there are exactly twelve disclinations can now be seen either by counting vertices, edges, and triangles under the constraint $V - E + F = 2$, or more generally because the total disclination charge must sum to 4π [43].

Between the disclinations are patches of regular six-fold lattice which has no topological freedom: thus, *the capsid is completely determined by the placement of the disclinations*. Since there may be hundreds of network vertices, and only twelve disclinations, this is in principle a simplification.

B. Hamiltonian

We represent the growing capsid as a number of approximately equilateral triangles connected along the edges. We then generalize the discretized Hamiltonian used by Lidmar et al. [33] to include spontaneous curvature θ_0 and binding and steric terms.

$$\mathcal{H} = \mathcal{H}_{\text{stretch}} + \mathcal{H}_{\text{bend}} + \mathcal{H}_{\text{steric}}. \quad (2.1)$$

1. Elastic energy

The first two terms in eq. (2.1) are elastic terms for bond stretching and bending:

$$\mathcal{H}_{\text{stretch}} = \frac{\sqrt{3}\tilde{Y}}{4} \sum_{\langle ij \rangle} (|\vec{r}_i - \vec{r}_j| - r_0)^2, \quad (2.2)$$

$$\mathcal{H}_{\text{bend}} = \frac{2\tilde{\kappa}}{\sqrt{3}} \sum_{\langle IJ \rangle} (1 - \cos(\theta_{IJ} - \theta_0)). \quad (2.3)$$

Here, $\langle ij \rangle$ denote pairs of nearest-neighbor vertex pairs with positions \vec{r}_i , and $\langle IJ \rangle$ denote pairs of nearest-neighbor triangles. The exterior dihedral angle $\theta_{IJ} = \cos^{-1}(\hat{n}_I \cdot \hat{n}_J)$ where \hat{n}_I is the unit normal to triangle I .

Our discrete parameters have the same dimensions as the two-dimensional Young’s modulus, Y , and bending rigidity, κ , which are emphasized in continuum approaches to predicting capsid shapes [33], and for a flat sheet in the linearized regime they have the same values. If we parameterized our model by spring constants K_{stretch} and K_{bend} equal to the curvature of our radial and angular potentials at the bottoms of their respective wells, we would have $\tilde{Y} = \frac{2}{\sqrt{3}}K_{\text{stretch}}$ and $\tilde{\kappa} = \frac{\sqrt{3}}{2}K_{\text{bend}}$. Evidently one elastic coefficient may be taken to define an energy scale — we chose units so that $r_0 = 1$ and $K_{\text{stretch}} = 1$ — and then only the ratio $\tilde{\kappa}/\tilde{Y}$ matters physically. We parameterized this by a *Foppl-von Kármán length*

$$\ell_f^2 \equiv \kappa/Y. \quad (2.4)$$

Previous work expressed the same ratio using the dimensionless Foppl-von Kármán number [33]

$$\gamma = YR^2/\kappa, \quad (2.5)$$

where R is the capsid radius which is well-defined in the case of a spherical capsid. For non-spherical capsids, a definition of R is problematic; and in any case, ℓ_f controls many other properties, such as the exponential decay of strain and Gaussian curvature with distance from a defect. Thus, we consider ℓ_f to be the more fundamental parameter and write $\gamma = (R/\ell_f)^2$. We note that a small ℓ_f corresponds to a large Young’s modulus and therefore is an *angular* (or faceted) regime. On the other hand, large ℓ_f entails a large bending stiffness and leads to a *smooth* regime.

2. Spontaneous curvature and steric repulsion

Microscopically, we expect that capsid proteins are more similar in shape to cones or pyramids than to cylinders. Therefore, if two proteins are in contact, the outer surface will be bent at a characteristic angle. This suggests that $\mathcal{H}_{\text{bend}}$ should favor some angle θ_0 . Additionally, it motivates our model of steric repulsion based on tetrahedra.

The preferred dihedral angle θ_0 is a key parameter since it is the main determinant of capsid size in our model, as was speculated to be the case in real capsids [16]. This corresponds to spontaneous curvature in a continuum model.

The final term $\mathcal{H}_{\text{steric}}$ in (2.1) is a steric potential, chosen to vanish for all physically realistic capsids. The steric potential proves difficult to incorporate into our cartoon model, for two reasons. Firstly, all the inter-unit interactions of properly bonded units should already be accounted for in the elastic term $\mathcal{H}_{\text{stretch}} + \mathcal{H}_{\text{bend}}$, so we demand that the steric force not make additional contributions to these forces. Secondly, the other terms in Eq. (2.1) relate units that are “topological neighbors”, as defined by the bond network (the discrete configuration). But two parts of the capsid which are distant topologically may grow to be nearby in real space (the positional configuration), and must then be kept from intersecting. Thus, the steric term must apply equally to topologically distant segments of the capsid, or to adjacent units, e.g. two as-yet unjoined triangles on the same vertex.

To implement a computationally tractable steric potential, we imagine each triangle to be a tetrahedron and add a repulsion between the apex of one tetrahedron and the vertices on the base of each other. This potential vanishes for physically realistic capsids. A more technical discussion may be found in Appendix B, and the steric Hamiltonian is defined in Eq. (B1).

3. Microscopic estimation of elastic energy

Interactions between capsid proteins have been simulated electrostatically [14] to determine binding energies for large multimers of capsid proteins, necessarily in different relative positions. Such simulations could be extended to determine the elastic constants for particular viruses with known protein structure.

Alternatively, we can perform a rough estimate of the elastic parameters by considering some experimental measurements. Ivanovska et al. [44] carried out mechanical structure measurements on the $T = 3$ phage $\phi 29$ and found the bulk modulus $B \approx 1.4\text{GPa}$, the thickness $t \approx 2.5\text{nm}$, and the radius $R \approx 25\text{nm}$. We obtain an estimate of the two-dimensional Young’s modulus by $Y \sim Bt \approx 3.5\text{N/m}$. We can determine the size of each unit, r_0 , by comparing the surface area of a sphere to the area of $20T$ equilateral triangles, $4\pi R^2 = 20T \frac{\sqrt{3}}{4} r_0^2$, so that $r_0 \approx \frac{1.2R}{\sqrt{T}} \approx 17\text{nm}$.

To get an idea of the elastic parameters for HIV, we can produce model capsids by hand which resemble HIV cores. In particular, we grew several capsids with about 500 triangles in a cone shape. Tuning the elastic parameters to roughly match the observed shape of HIV [27], we found $\gamma \approx 550$ produces the correct amount of facetedness. This corresponds to $\ell_f = 0.16r_0$. Using the results presented in Sec. IV A, we can also guess a value for $\theta_0 \approx 20^\circ$, which is actually rather large.

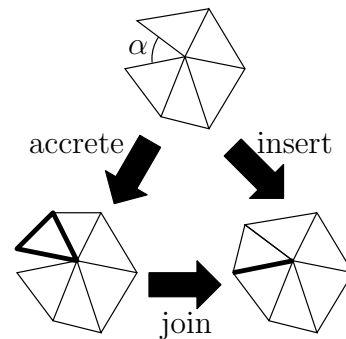


FIG. 2: Elementary growth steps of *insertion*, *joining*, and *accretion*, performed from the same starting point of an edge with opening angle α . Insertion can be decomposed into Accretion followed by Joining.

Given a set of connected triangles, we can now use this Hamiltonian to determine the lowest-energy configuration of the positions of the triangles. These positions correspond to a continuous degree of freedom which is now fully determined by the model (\mathcal{H}) and the connectivities – the discrete degree of freedom. Ultimately, we are only concerned with the discrete configuration.

C. Growth

We have noted that capsids are determined by the locations of the disclinations (pentamers). For an irreversible growth model, in which no step can be undone, the fundamental question is therefore: while growth occurs at the border, which twelve vertices are frozen in as pentamers? Keeping this in mind, we will now discuss our capsid growth process.

1. Growth steps

We define transitions between incomplete capsids, consistent with irreversible growth, called *growth steps*. Two elementary growth steps are immediately apparent: *accretion* and *joining*. Accretion is the addition of a single triangle to a border edge and joining is the formation of a bond between two adjacent border edges. We require the vertex between these two joined edges to have five or six triangles around it in order to ensure that only pentamers and hexamers form.

Besides accretion and joining, we define a third, composite growth step: *insertion*. We define insertion as accretion followed by joining along an edge of the new triangle. The vertex into which we insert must have four or five triangles. Insertion at a 4-vertex or joining at a 5-vertex is the only way to form pentamers. These three steps are illustrated in FIG. 2.

Growth begins with a small template – either a single triangle or a pentamer of five triangles about a vertex.

From here, the growth is determined by the sequence of growth steps, which is chosen stochastically. We will first present our rules for the relative probability of choosing the growth steps, and then explain their microscopic rationalization.

2. Rates

We precede each growth step by relaxing all vertex positions using a conjugate-gradient algorithm to minimize the positional energy \mathcal{H} . Now a rate k_ν is defined for each allowed growth step ν , which is a function of the local topology and of the *opening angle* α between pairs of edges at each vertex on the border, defined in FIG. 2. The probability of step ν is then taken to be $k_\nu / \sum_\mu k_\mu$; once a ν is picked, we perform the step and iterate the process (beginning as before with a relaxation).

We take the accretion rate, k_A , to be independent of the local configuration: in particular it is not a function of α .

So long as we are concerned only with the outcome and not the time taken to reach it, only relative rates are relevant. Thus we can now define

$$\frac{k_J(\alpha)}{k_A} = \Gamma_J e^{-\alpha^2/2\sigma^2} \quad (2.6)$$

$$\frac{k_I(\alpha)}{k_A} = \Gamma_I e^{-(\alpha-\pi/3)^2/2\sigma^2}, \quad (2.7)$$

with justification to follow. Note that steps are only considered if (1) they do not break any topological rules by enclosing a non-pentamer/hexamer, and (2) they do not lead to steric hindrances. This second point is discussed further in Appendix B.

3. Microscopic justification of rates

While many models explicitly account for units in solution and fluctuations in incomplete capsids [20, 39], we have chosen a simplified cartoon model. Implicit to this is the idea that the capsid is thermally fluctuating between growth steps.

Say the time between successive additions is longer than the relaxation time scale of the positional degrees of freedom, Then between each growth step, we can assume that the incomplete capsid is in equilibrium and thus samples a Boltzmann distribution. We consider the energy of fluctuations about the relaxed position. For a particular vertex, i , with relaxed opening angle α_i , the energy of a fluctuation with opening angle $\alpha_i + \Delta\alpha_i$ is well approximated by a quadratic, so that

$$\Delta E(\Delta\alpha_i) \approx \frac{1}{2} A_i (\Delta\alpha_i)^2. \quad (2.8)$$

We can therefore determine the elastic energy barrier for a vertex to have an angle favorable for either insertion

($\alpha_i + \Delta\alpha_i \approx \pi/3$) or joining ($\alpha_i + \Delta\alpha_i \approx 0$), and thus the transition rates, $k_I(\alpha_i)$ and $k_J(\alpha_i)$, respectively. It is now clear that the rates defined above in Eqs. (2.6)-(2.7) are merely Arrhenius factors, with

$$\sigma^2 = \frac{k_B T}{A_i}. \quad (2.9)$$

Note that T here is temperature, and should not be confused with the triangulation number defined earlier.

During any growth step, new bonds are formed. We may consider an extra energy term, $\mathcal{H}_{\text{bind}} = -N_b E_b$, contributing a binding energy $-E_b$ for each of the N_b bound edges in the capsid. Such an energy is independent of the positional configuration. For our irreversible model to satisfy detailed balance, we need $E_b \gg \Delta E(\Delta\alpha_i)$ so that the energy barrier for the reverse transition is large compared to that for the forward transition.

The parameter A_i and therefore σ depends not only on the elastic constants, but also on the local environment of the vertex in the capsid. We can determine normal values for A_i by varying angles on different capsids with different energy parameters, and twice differentiating the Hamiltonian about the minimum. Because most of the opening angle fluctuations in physical situations are *in-plane*, A_i depends most strongly on the Young's modulus, and generally

$$A_i = \frac{\partial^2 \mathcal{H}}{\partial \alpha_i^2} \approx 0.1 \tilde{Y} r_0^2. \quad (2.10)$$

(Note that this is an absolute dependence on the energy scale \tilde{Y} , and is the only reference we will make to an absolute energy, since everything else depends only on the ratio $\tilde{\kappa}/\tilde{Y} = \ell_f^2$.)

We can perform a rough estimate of this width now using the elastic parameters estimated for $\phi 29$ in Sec. II B we find $A_i \approx 0.1 Y r_0^2 \approx 630 \text{eV}$. We therefore expect fluctuations of

$$\sigma = \sqrt{\frac{k_B T}{A_i}} \approx .0064 \approx .37^\circ \quad (2.11)$$

at room temperature $T = 300 \text{K}$. This is much less than the value of $\sigma \approx 10^\circ$ we will need for satisfactory growth. However, this estimate was based on measurements from the head of a mature bacteriophage which is observed to be much more faceted (small ℓ_f , large Y/κ) than the immature form in which assembly occurs. Such small fluctuations are probably important for stability and infectivity, but also quite detrimental to growth [45]. As such, we expect the immature capsid to have much larger fluctuations, although no mechanical studies have been done to allow this determination.

Sometimes a deterministic growth rule is preferred to the stochastic rule presented above. One possibility is a rule which accepts only the move with the largest rate at any given point.

III. FAILURE MODES

The restriction that all vertices have either five or six triangles can lead to problems in irreversible growth. It is entirely possible for a growing capsid to perform a wrong growth step resulting in a state which can never be completed – that is, no complete capsid satisfying the pentamer/hexamer-only requirement includes the particular incomplete capsid in any of its possible growth histories. This section surveys the two common failure modes. A common theme is that the failure can be identified non-locally, long before a step is reached at which the growth rules break down; a more rigorous treatment is given in Appendix A.

We cannot avoid considering failures, since we must exclude them when reporting statistical distributions of the resulting capsid ensemble (see Sec. IV). More importantly, we have taken for granted that the actual assembly has a high success rate (say, 10% to 99%). Indeed, most of our labor on the project reported in this paper consisted of locating the parameter space in which assembly had a high success rate. Classifying the failure modes is a prerequisite to understanding what conditions make them rare.

Failure modes are also experimentally pertinent. Whatever the “ideal” capsid is for a given virus species, there is likely to be more than one possible assembly model that produces it. But since different models will tend to fail in different ways, they are better distinguished experimentally by study of defective rather than of ideal capsids. If there are virus species which grow their capsids near the limit of complete irreversibility, the resulting ensemble is bound to contain mistakes. Indeed, HIV cones have been observed that are surrounded with what is believed to be a second sheet of the protein-unit triangular network [27].

A. Unfillable quadrilateral hole

First we look at a failure which occurs only at the end of a growth process. FIG. 3(a) shows a common configuration with a single quadrilateral hole. Parallel transporting a vector around the border gives no rotation and therefore there is no net disclination inside (the net “disclination charge” is zero. – recall the discussion in Sec. II A) The only conceivable filling is to by two triangles, but either possibility introduces a 7-coordinated vertex [46].

A less trivial example of this situation is shown in FIG. 3(b). Here we can parallel transport a vector around the border to see that a single disclination must reside within the border; however, there is no way to fill in the remaining triangles to satisfy this. See Appendix A for a more rigorous discussion of this phenomenon. If we continue growth, the hole will eventually shrink to something similar to FIG. 3(a). Some believe that such a hole is not detrimental to capsids, and in fact capsids are known to

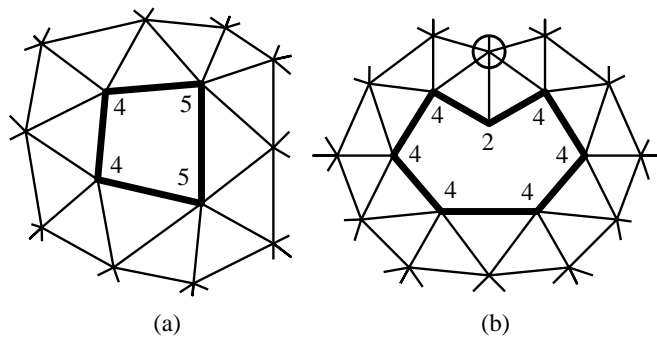


FIG. 3: Incompletable holes at the end of growth. Neither hole can be filled without introducing a heptamer. The hole in (b) would have been avoided had the circled vertex been made a pentamer

be permeable to water and ions.

This type of failure was common in all the growth rules we considered, although it is more prevalent in certain situations. In particular, if $\sigma \gtrsim 20^\circ$ or $\Gamma_{I,J} \gtrsim 200$, then creation of pentamers becomes very random and is no longer based much on the geometry. In normal growth, particularly at small ℓ_f , local strains cause angles along the border to suggest whether a pentamer or hexamer should be created, but large σ dulls the sensitivity to this.

B. Crevice formation

Next we look at a failure which can occur at any point during the growth, called a *crevice*. We see in FIG. 4(a) a portion of a border with the four labeled vertices in a characteristically incompletable configuration. This becomes clear when the border is flattened onto a reference lattice, as seen in FIG. 4(b). We now see that in the absence of pentamers in the neighborhood of this section of border, several triangles lay on top of others. The introduction of a pentamer can only make matters worse. By effectively cutting out a 60° section of the plane, it becomes even more crowded. The only way to alleviate this self-intersection is by introducing a heptamer or other negative disclination.

Crevice failures can occur in different regimes, but arise in particular during *fingered* growth. If accretions are much more common than both joinings and insertions (such is the case when either $\sigma \lesssim 5^\circ$ or $\Gamma_{I,J} \ll 1$), then we expect many long fingers only one or two triangles wide. Crevices occur easily between these fingers. Even in the absence of fingers, sometimes creating a pentamer will distort a neighboring vertex enough that the angle is too large for insertion or joining. This too often results in a crevice.

Say just one single crevice failure occurs during growth. Further growth outward from the failure should be prevented by steric hindrance. But growth elsewhere along the border will continue and eventually fill in the crevice

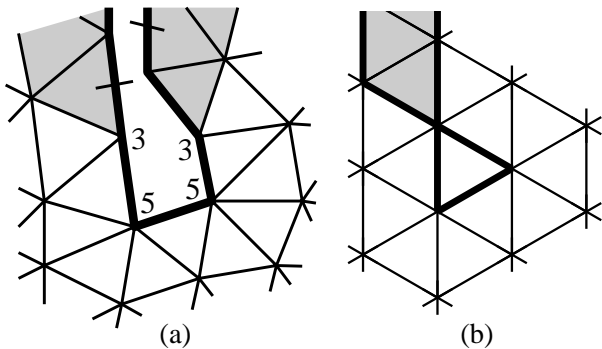


FIG. 4: (a) An incompletable configuration. The sequence of vertices with 3, 5, 5, and 3 triangles on a border can never lead to a valid complete capsid. Joining the marked edges would produce an unfillable quadrilateral hole, similar to FIG. 3(a). (b) The same border flattened onto a triangular reference lattice. The shaded triangles from (a) now overlap the corresponding triangles from the opposite side.

from its far end. Then the capsid will almost complete, leaving a small hole of the same type discussed in Subsec. III A above. The two marked edges in FIG. 4(a), for instance, might join leaving a quadrilateral hole.

If two or more crevice failures occur, however, our model’s resulting capsid will have a network of cracks connecting all these failures. because Real capsids might repair this problem by binding some binding of edges not sharing a vertex (which is forbidden in our model); in that case, the final result might instead have several small quadrilaterals of the type seen in FIG. 3(a).

Although it is not as obvious, the smaller holes presented in Sec. III A also have borders whose flattened images intersect themselves when cut at certain places. We can generalize this by stating that a border is incompletable if there is any choice of cut which leads to the flattened border, along with its incident triangles, intersecting itself, then the border is incompletable. The converse is almost always true as well.

C. Failure rates

If 5-fold vertices were simply incorporated at random moments during the growth, virtually every capsid would fail in one of the two modes described in this section. Since the topological constraints to be satisfied are non-local, and the growth rate depends on local properties, it seems mysterious at first how the growth can be as successful as it is. The key is that, in an elastic medium, the strain due to a defect (such as a disclination) is also non-local; at least, it decays as a power law with the distance from the defect. In this fashion, the necessary information about the locations of faraway disclination is passed to the growth border.

Since growth is stochastic, there is a possibility of errors despite this passage of information. All capsids are

in danger of making an error after the eleventh disclination is in place, and many are in danger even earlier.

We can model the failure probability with a very simple assumption: each time a triangle is added, there is a fixed probability $p_c \ll 1$ of starting a crevice. This is not intended quite literally: p_c must be understood as the fraction of edges along the border which can possibly start a crevice, times the probability on each such edge that this “wrong” step will be taken when a triangle is added there. (The crucial step might be a “joining” but this contribution gets folded in with the other one, since the border settles into a dynamic near-steady state, so that the ratio of step types will be uniform on average.)

The survival probability of a defect-free capsid is thus

$$\frac{dP_{\text{sur}}}{dN} = -p_c \quad (3.1)$$

where step N plays the role of time, so that

$$P_{\text{sur}}(N) \propto e^{-p_c N}. \quad (3.2)$$

Growth will terminate after all twelve disclinations have been incorporated, i.e. on average when $N = \bar{N}(\theta_0, \ell_f)$ (the mean size of capsids formed as a function of the parameters). Furthermore, we hypothesize that $p_c \approx p_c(\ell_f)$, i.e. crevice formation depends strongly on the ratio of elastic constants almost not at all on the preferred angle θ_0 . If so, the probability of success is

$$P_{\text{succ}} = P_{\text{sur}}(\bar{N}) = e^{-p_c \bar{N}}. \quad (3.3)$$

IV. RESULTS

Here we discuss several measurements which can be used to quantitatively characterize various properties of capsids (individual, or as an ensemble) specified by a triangulation of vertices, such as the results of our growth model. We concentrate on measures which could be implemented on data from cryo-EM experiments, namely size distribution, facetedness, and Gaussian curvature.

Fig. 1 shows an example of a typical capsid shell resulting from our growth simulation. This capsid emphasizes that our configurations are inherently random and irregular. The degree of “lumpiness” in the external shape depends strongly on the Foppl-van Kármán ratio γ , as is elaborated in Sec. IV C, below.

Each capsid is grown until either a successful completion, or an identifiable failure, such as a self-intersection in the flattened border. Relaxations are minimized until the gradient-squared is less than 10^{-6} , in units with $K_{\text{stretch}} \gtrsim K_{\text{bend}} = 1$. The entire growth process for a small capsid takes several minutes on a 1.6GHz processor, while a large capsid takes many hours, the majority of the time devoted to minimizing energy. The following plots of size and success rate include data from 3818 capsids.

A. Size

The simplest thing to observe about a capsid is its size. We can count the number of triangles N , or measure the average radius R . Even for incomplete capsids, a least-squares fit to the surface of a sphere can yield a radius of best fit. As expected [13, 16], capsid size depends most heavily on two dimensionless parameters from our effective Hamiltonian, $\ell_f = \sqrt{\kappa/Y}$ [47] and θ_0 . The latter parameter could be converted into a length scale,

$$\ell_\theta \equiv \frac{r_0}{2\sqrt{3}} \cot(\theta_0/2). \quad (4.1)$$

This length is the radius of curvature from two equilateral triangles with side length r_0 joined at an angle θ_0 and tangent to a common sphere. In the smooth regime, when $\ell_f \gtrsim \ell_\theta/50$, the variation in the dihedral angles at different bonds is small, so the radius of the resulting capsids tends to ℓ_θ . For smaller ℓ_f (the angled regime), the Young's modulus increases. Hexamers, which make up most of the capsid, become flatter. Thus, the effective preferred angle θ_0^{eff} decreases, resulting in larger capsids. Additionally, the energy cost of disclinations increases, which may increase capsid size in some models [13]. We plot r_0/\bar{R} versus $r_0/\ell_\theta = 2\sqrt{3}\tan(\theta_0/2)$ in FIG. 5 for several different values of ℓ_f^2 . We see that, for small $\gamma = (R/\ell_f)^2$, the curves are roughly parallel to, and slightly less than the line $r_0/\bar{R} = r_0/\ell_\theta$, and the distance from this line increases as $\gamma \propto (r_0/\ell_f)^2$ increases. Notice that we can clearly see two different regimes in this plot. The $(r_0/\ell_f)^2 = 10$ curve in particular seems to change behavior near $\bar{R} \approx 4r_0$, corresponding to $\gamma = (R/\ell_f)^2 \approx 160$. This is suggestive of a buckling transition [33]. We can get a glimpse behind these curves in FIG. 6, which shows the average number of pentamers as a function of N , broken out into different values of θ_0 .

Because most of the larger capsids failed, we used the best-fit radius for any capsids with at least 9 pentamers at the time of failure. Also, very small (< 100 triangles) capsids were removed from the averages for $(r_0/\ell_f)^2 \geq 100$, because they were an artifact of too large a width σ in the growth rules.

B. Success rate

An important consideration for an irreversible growth model is under what circumstances it successfully produces complete capsids. We have already shown that a variety of failure modes exist, resulting in incompletable capsids. We can easily quantify how often these failures actually occur as a function of parameters. We predicted in Sec. III C that the success rate should be exponential with the expected size of the capsid. We can find a linear fit between $1/\bar{N}$ and $\cot^2(\theta_0/2)$, very similar to FIG. 5. Using this fit, we map the parameters θ_0 and ℓ_f to

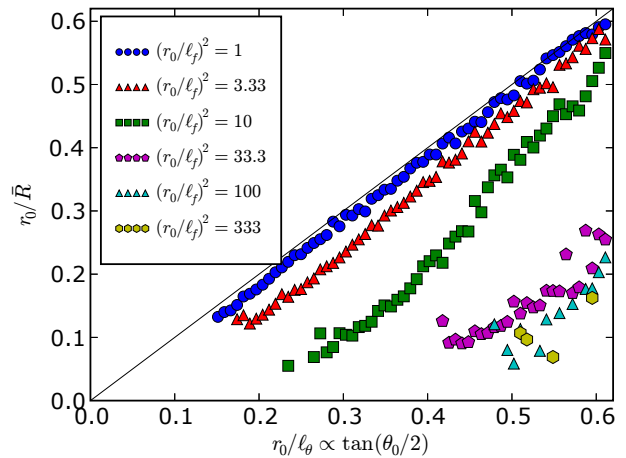


FIG. 5: Plot of r_0/\bar{R} versus $r_0/\ell_\theta = 2\sqrt{3}\tan(\theta_0/2)$. We see that in the smooth regime of large ℓ_f , the radius R of the grown capsids approaches ℓ_θ from above. In the angled regime (small ℓ_f), the data are more erratic. Note that if the linear trends continue, \bar{R} diverges at finite θ_0 . Since this cannot happen, the linear behavior must break down somewhere.

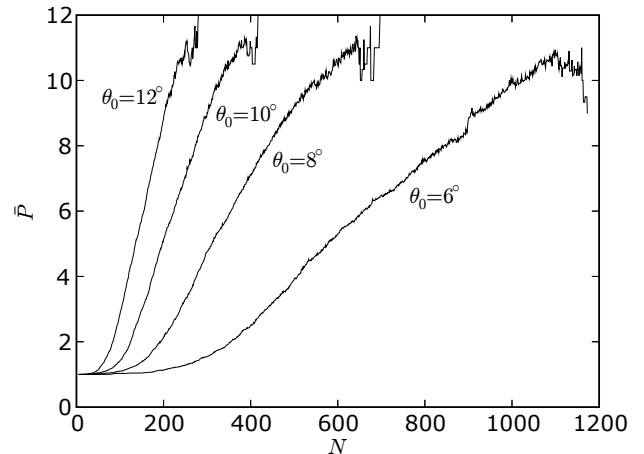


FIG. 6: Plot of the average number of pentamers \bar{P} versus the number of triangles N . This gives a picture of the general pathway of growth behind the curves in FIG. 5. This growth was carried out at $(r_0/\ell_f)^2 = 1.3$, and different spontaneous curvatures θ_0 are shown in the figure. We see that growth consists of a long time spent at $P = 1$, followed by a rather linear regime in which $d\bar{P}/dN$ is roughly constant. Note that both the initial time at $P = 1$ and the following slope depend on ℓ_f .

N_{expected} and plot the percentage of capsids that completed successfully when grown with this set of parameters. FIG. 7 shows that the exponential decay constant depends strongly on $vk\ell$ but is largely independent of θ_0 .

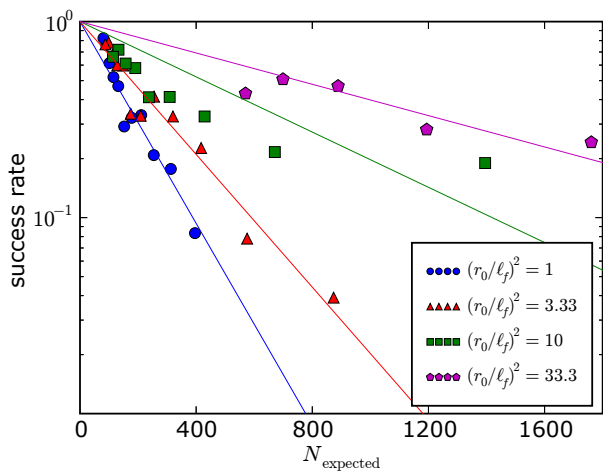


FIG. 7: Distribution of success rates as a function of N_{expected} , fit from the size measurements. Data with $N_{\text{expected}} < 0$ or $N_{\text{expected}} > \max(N_{\text{observed}})$ were thrown out. $N_{\text{expected}} < 0$ corresponds to a different regime in which the fit fails. We see exponential decay, suggesting that introduction of errors is a Poissonian effect, as discussed in Sec. III C.

C. Shape

Beyond size and success, most other measurements fall under the category of shape measurements. In particular, we might measure either the degree of symmetry or the facetedness of a capsid.

Spherical harmonics may be useful for evaluating icosahedral symmetry, as spherical harmonic coefficients of icosahedrally symmetric functions vanish for all but $\ell = 0, 6, 10, \dots$

Kingston et al. [30] uses the asphericity, defined as the ratio of inradius to circumradius to measure the faceted shape of RSV capsids. Lidmar et al. [33] also defined an asphericity, $\langle R^2 \rangle / \langle R \rangle^2$. While these are good measurements for symmetric capsids, they are not useful for the irregular capsids we grow, because they cannot distinguish between, for instance, a smooth egg-shaped capsid and a faceted spherical capsid. We instead use a measure based on the Gaussian curvature, described below.

1. Curvature

In light of recent advances in tomography, a very relevant measure is Gaussian curvature K . In our discrete triangular model, we can measure the integrated Gaussian curvature $I = \int K da$ over the neighborhood nearest to a single vertex by measuring the area (equivalently, angle surplus) of the spherical polygon traced out by the incident triangles' unit normals. We can easily extend this to the integrated curvature over all the vertices within any loop around the capsid. The integrated curvature over the entire capsid is always 4π , a topological invari-

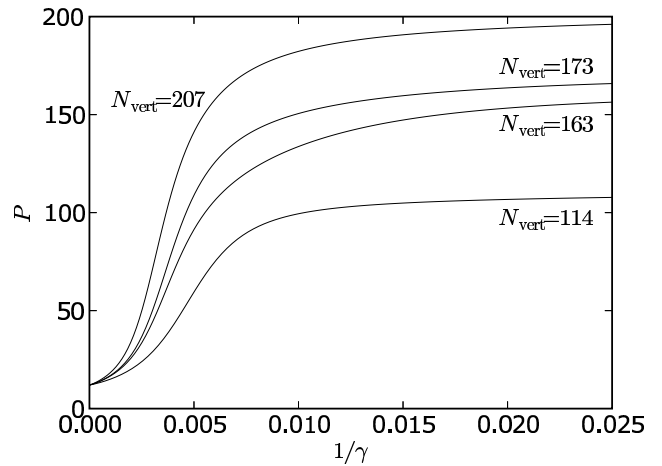


FIG. 8: Inverse participation ratio for four capsids with different numbers of vertices N_{vert} . We can see that as $\gamma \rightarrow \infty$ (the angular limit), $P = 12$, and as $\gamma \rightarrow 0$ (the smooth limit), $P \rightarrow N_{\text{vert}}$. The exact shape depends on the placement of pentamers, but we see generally an inflection point between $\gamma = 100$ and $\gamma = 200$.

ant related to the Euler characteristic. The question then arises how this curvature is distributed over the capsid. For highly faceted capsids, each pentamer has $I \sim \pi/3$, while the rest of the capsid has $I \rightarrow 0$. On the other hand, the curvature is distributed uniformly over smooth capsids. This motivates the definition of an inverse participation ratio (IPR),

$$P = \frac{(\sum_j I_j)^2}{\sum_j I_j^2} = \frac{(4\pi)^2}{\sum_j I_j^2}, \quad (4.2)$$

where I_j is the integrated curvature about vertex j . This essentially measures the number of lattice sites the curvature is localized to. The IPR is plotted for a single capsid relaxed to different elastic parameters in FIG. 8. We see that $P = 12$ at $\gamma \rightarrow \infty$ while $P \rightarrow N_{\text{vert}}$ at $\gamma \rightarrow 0$.

This same integrated curvature can be measured on triangulated tomographical data from capsids. The integrated curvature within large loops should be relatively stable even if the Gaussian curvature varies quickly. For an arbitrary loop around a capsid, we will get a contribution of $\pi/3$ from each enclosed pentamer. The loop may then be pulled tighter to pinpoint the location of each pentamer. We simulated this process by growing a large number of random capsids and integrating the curvature within many random loops on each. Each capsid was relaxed to several different values of γ . The resulting distribution of curvatures is displayed in FIG. 9. At large $\gamma = 50000$ we see very sharp peaks. These peaks diffuse into a mostly uniform background by $\gamma = 500$.

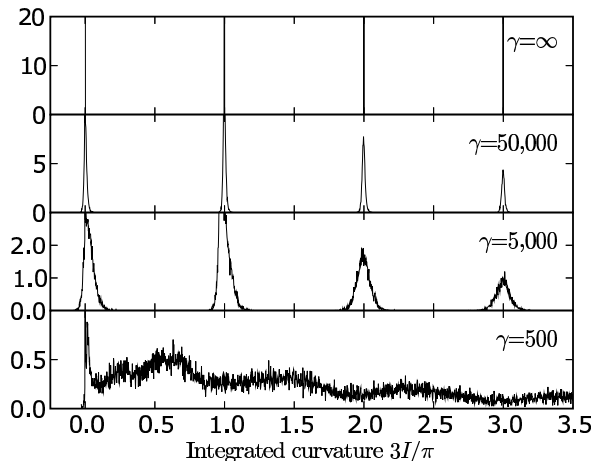


FIG. 9: Distribution of integral curvatures within random loops around random capsids relaxed to different elastic parameters. The distribution is sharply peaked at the integers for large γ and diffuse for small γ .

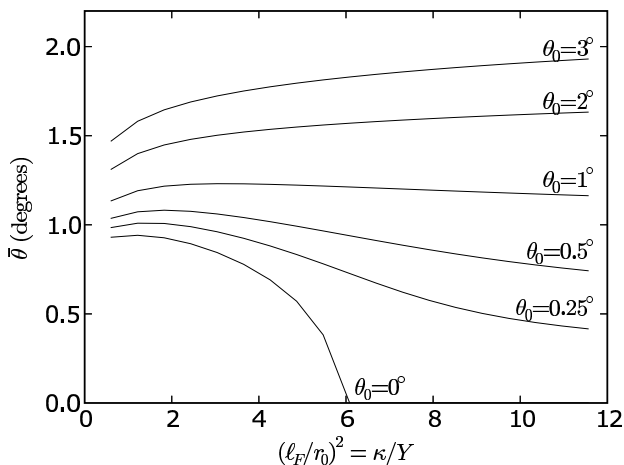


FIG. 10: Average dihedral angle of a large pentagonal sheet with a single disclination in the center. Plotted versus ℓ_f at different θ_0 . The bottom $\theta_0 = 0$ curve shows a first-order buckling phase transition. Each subsequent curve increments θ_0 by 0.25° .

2. Average dihedral angle

We can measure the average dihedral angle of either a growing or a complete capsid. FIG. 10 shows a graph of the average dihedral angle for a very large pentagonal sheet with a single disclination in center as a function of ℓ_f , at different θ_0 . We see a first order phase transition at $\theta_0 = 0$, and curves generally reminiscent of $\langle M \rangle$ versus T plots of the Ising model at different H .

V. DISCUSSION

In this section, we recapitulate the highlights of our model and the simulation results, and outline extensions that could improve their realism.

A. Summary of results

Our irreversible growth model, based on trimer units with the simplest possible Hamiltonian and growth rates, did succeed at producing closed capsids, but only when the parameters are tuned to the proper range.

Our model (Sec. II) made a sharp division between configuration variables that were continuous (position) and discrete (bonding topology); correspondingly the model parameters were divided between a Hamiltonian (harmonic form) and rate constants for a set of first-order processes; for simplicity, monomers in solution were not treated explicitly. The choice that most shaped this work was to use trimer units (triangles), which turns out to have several inherent disadvantages. First, our “insertion” step (Sec. II C) was redundant; unfortunately, omitting this (relying on the “joining” step in its stead) produces failures – the fingered growth and crevices elaborated in Sec. III B. In other words, good growth depended on joinings being rare compared to insertions, which followed from our growth rules (Sec. II C), since opening angles α near 0° are much less common than those near 60° . Perhaps this means that if a capsid assembles from trimers in solution, the only way to have normal growth is that there must be cooperative binding in 60° angles.

Our results may be divided into two categories: the growth process (including the success rate) and the shape of the resulting model capsids. In the first category, we found mathematical descriptions (Appendix A) which clarified the constraints on the positions of the fivefold-coordinated vertices which fully characterize the bond network. Additionally, we uncovered simple equations characterizing the dependence of the capsid’s final size on the preferred angle θ_0 , Eq. (4.1), and of the failure rate on capsid size, Eq. (3.3). In the second category, we extended the concepts of Ref. [33] to irregular capsids. In particular the ratio of bending and stretching stiffnesses – which we suggest is best parametrized by a length, Eq. (2.4), rather than a dimensionless ratio – controls whether the resulting shape is smooth or angular, as we have characterized by an inverse participation ratio, Eq. (4.2).

B. Future directions: more realistic random growth

1. Models with non-trimer units?

The retroviruses we claim to model have distinct dimerization and hexamerization domains, but no trimer

domains have been observed in retroviral capsids. A model based instead on pentamers and hexamers could be implemented simply by changing the growth steps to add several triangles at a time, such as to fully enclose a single vertex each step into either a hexamer or a pentamer. We gain some benefit, however, from actually changing our representation to a honeycomb lattice – the dual to our current triangular lattice. Vertices of the dual lattice are all three-coordinated, so each vertex along the border has either one or two capsomers attached to it – much simpler than the five different possible coordination states for border vertices in the trimer model. In this model, growth rules could explicitly depend on the total coordination of a vertex. Such coordination-based rules greatly assisted successful growth in our trimer model, but were not as physically justifiable as they are in the dual model.

These considerations suggest that behavior arising from this choice is not universal. We expect models based on dimers, trimers, or pentamers and hexamers to fall into different universality classes.

Another direction leading to a more realistic model is to improve the accuracy of our interactions. Microscopic electrostatic simulations, such as with the CHARMM software, could provide a more realistic Hamiltonian for specific viruses, which could be included in future models.

2. Lattice fluctuations

A deeper understanding of the relationship between topological configurations is critical. So far we have only thoroughly considered irreversible growth transitions. Other transitions relate to the motion of disclinations on the lattice (always in pairs), both for the purpose of enumerating the near-symmetric states, and for an understanding of the rearrangement dynamics by which real capsids may anneal their bond configurations into the free energy minima predicted by many equilibrium models.

C. Future directions: realistic shapes

All well-studied real capsids exhibit greater regularity than our current model can regularly generate. How can the Hamiltonian (or the growth dynamics) be modified so as to generate an icosahedral, or (for HIV) conical capsid?

1. Icosahedral symmetry

The main challenge for theory is to explain the assembly of icosahedrally symmetric capsids, if one is not close to equilibrium. Hamiltonians such as ours do indeed give effective repulsion between the disclinations, and the free

energy minimum is known to have icosahedral symmetry in similar models [13, 33]. However, this is simply insufficient to produce large symmetric capsids in a model where the accretion rate depends on local geometry, since the growing border does not contain enough information in just the opening angles (Sec. II C). Even deterministic variants of the growth model never yielded icosahedral capsids larger than $T = 4$.

We speculate that if the bending potential $\mathcal{H}_{\text{bend}}$ was not simply harmonic around θ_0 , but instead had minima at two different angles θ_1 and θ_2 , this might robustly favor a regular pattern of edges with θ_1 and θ_2 , thus permitting determination of larger icosahedral capsids. A double-well potential would presumably represent some sort of conformational switch, perhaps an internal bending between two domains of the capsid protein. Thus, this proposal has some features in common with the matching-rule models that we dismissed as implausible (Sec. I B), but anharmonic potentials seem much more natural than variations in the edge-binding (which, in our model, corresponds to the term $\mathcal{H}_{\text{bind}}$ mentioned briefly in Sec. II C).

2. Retroviruses

We asserted that the randomness of our model's growth behavior makes it appropriate for modeling the irregular capsids of retroviruses such as HIV. However, HIV capsids do have a typical gross shape, which is conical in vivo (sometimes tubular in vitro), whereas our current model grows round capsids on average. A cone is characterized by having (say) five disclinations around its smaller end, seven around the large end, and none on the belt in between; this means the rates of adding pentons must somehow vary during different stages of the growth. When cones form inside an envelope, the difference could be attributed to depletion of the monomers as they are incorporated into the capsid: that (see Sec. II C) would decrease the rate of insertion but not of joining, leading to a greater chance of penton formation. A difficulty with concentration control is that cone completion leaves in solution 70% [24] of the capsid proteins: in order for this to grossly affect the rates, accretion must microscopically be a rather high-order process. It also leaves unexplained the large density of pentons at the *earliest* stage: a possibility is to add a simple interaction between the capsid and either the nucleic acid or the membrane [26, 27].

Acknowledgments

We would like to thank John Briggs for access to his unpublished work, and Robijn Bruinsma, Grant Jensen, Diana Murray, Boris Shraiman, and Volker Vogt for many discussions. This work was supported by U.S Dept of Energy grant No. DE-FG02-89ER-45405.

APPENDIX A: COMPLETABILITY

It is possible to grow an incomplete capsid which is not part of any allowed capsid. This appears to be a consequence of our rule that a capsid vertex can only have coordination 5 or 6. (Seven-coordinated vertices, were they allowed, would let the capsid recover from almost every “mistake” discussed in this section.)

As a complement to the more qualitative discussion in Sec. III, this appendix presents the technical criteria we discovered to identify when a partial capsid is or is not completable, non-locally and long before the growth rules carry us to a point where we must make a 7-fold vertex or stop. The completable conditions are defined entirely in terms of the growing border, which can be uniquely described by traversing the vertices (in a specified direction) and listing the number of triangles present at each vertex. Thus a string of numbers from 1 to 5 specifies a border. (6 is allowed, but is trivial.)

1. String representation

We can represent any border by a word $a_1a_2\dots a_n$, where $1 \leq a_i \leq 6$ is the number of triangles around the i^{th} vertex, counting clockwise from an arbitrary starting point. We define several operations on these string representations. First consider a cycle operation, $C(a_1a_2\dots a_n) \equiv a_2\dots a_na_1$. Because of the unimportance of the starting point in representing a border, this operation leaves borders invariant. We can also define $A(a_1a_2a_3\dots) \equiv (a_1+1)1(a_2+1)\dots$ and $J(a_1a_2a_3a_4\dots) \equiv (a_1+a_3)a_4\dots$, representing accretion and joining, respectively. Note that the a_2 term disappears upon applying J . This vertex is enclosed and is no longer part of the border. We therefore require $a_2 = 5$ or $a_2 = 6$. We can further define insertion $I = J \circ C \circ A$ as the composition of joining and accretion. Since these operations are sufficient to grow any capsid, we can uniquely describe a capsid by the sequence of operations on the border required to arrive at the border from a single triangle, 111.

Using this representation we can immediately identify some borders which are incompletable. Consider the border $X = 555\dots$. Joining is illegal since it leaves a vertex with 10 triangles. Accretion leads to $A(X) = 6166\dots$ which clearly cannot be completed since only joining can be done on the 6’s, and this leaves seven triangles about at least one vertex. Finally, insertion yields $I(X) = 66\dots$ which is incompletable for the same reason.

Any border which intersects itself on a flat reference lattice is incompletable (coincident edges are allowed). It is important to take notice of which side of the border is the inside (from which the triangles are being counted) and which is the outside.

We thus define the complement of a border $\overline{a_1\dots a_n} \equiv (6 - a_n)\dots(6 - a_1)$. If the original border enclosed d disclinations then its complement encloses $12 - d$ and can

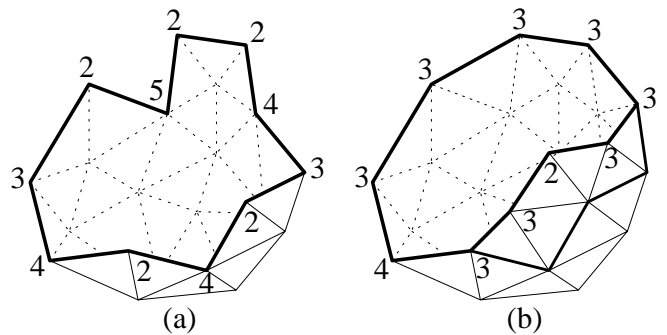


FIG. 11: Adding triangles to a $W = 0$ border (a) to transform it into the self-complementary form 3^m23^n4 seen in (b).

be glued together to form a complete capsid. We must note two things. Firstly, the complement of a border may be a border which cannot possibly be grown using our growth operations. Secondly, the complement is only unique insofar as the seam between the two incomplete capsids is occupied only by six-fold vertices. However, many “pseudo-complements” may be constructed which leave disclinations on this seam.

While the border by itself is useful for analyzing completable, it does not uniquely describe the interior. As we will see, pentamers (disclinations) can move without changing the border.

2. Winding number

We can compute the winding number $W(a_1a_2\dots a_n) \equiv \sum_i (a_i - 3)$ of a border, which is the number of 60° turns undergone by a direction which is parallel transported about the border. The total net number of disclinations within the border is $W + 6$. If we allowed seven-fold disclinations, they would be subtracted from this number. Since we only allow single positive disclinations, we can conclude that the winding number around any path on a valid capsid must be between -6 and $+6$, leaving $6 - W$ disclinations which must be placed in the unfilled part (the other side of the border, counting the vertices on the border itself).

3. Six disclinations remaining

We will now show that any border with winding number $W = 0$ which does not intersect itself on a flat reference lattice is completable by applying a finite number of growth operations to the border, resulting in a self-complementary border of the form 3^m43^n2 , which can be glued onto a copy of itself to make a complete capsid.

First draw the border on a flat reference lattice. It is now clear that triangles can be added to the border to transform it to the required form. So any capsid with a non-intersecting border and $W \leq 0$ is completable.

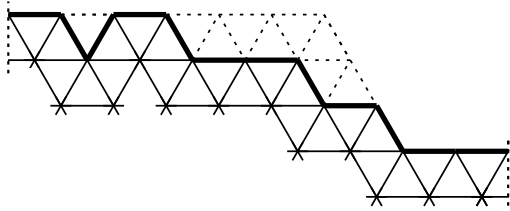


FIG. 12: An alternate point of view of the same procedure as illustrated in FIG. 11. We flatten the border onto a flat triangular reference lattice. The dashed lines on the left and right correspond to the place the border has been cut. That $W = 0$ is evident because there is no net rotation after traversing the border. It is also clear that adding the dashed triangles results in the same $3^m 23^n 4$ border as above.

This procedure is demonstrated in FIGS. 11 and 12

4. Late stage completability

When $W > 0$, there are more constraints. We can no longer add triangles freely since every row we add is smaller due to the enclosed disclinations. We will begin by considering the case of an incomplete capsid with eleven disclinations enclosed, leaving a deficit of one disclination needing to be placed.

a. One disclination remaining

In this case we can easily look at the reverse picture. If the border is completable then it is a path on a valid complete capsid and we can therefore look for a pseudo-complementary border to fill it. We can represent a triangular lattice with a single disclination as a flat triangular lattice with a 60° section cut out and the edges identified. If we therefore flatten our border onto a flat lattice, we expect the first and last points to be identified by this edge and therefore we can draw an equilateral triangle with the third point at the required location of the disclination. While the edges of the triangle need not be along a lattice direction, the third point is necessarily on the lattice. The border is completable if and only if this disclination is at an unoccupied point (outside of the original border). Note that because the border has a 60° rotation, this point is unique, regardless of the choice of starting and ending point. This process is demonstrated in FIG. 13.

b. Two disclinations remaining

Two disclinations ($W = 4$) works in a very similar way to the single disclination discussed above, except we have a 120° - 30° - 30° isosceles triangle instead. This gives a single charge $+2$ disclination, but since we do not allow

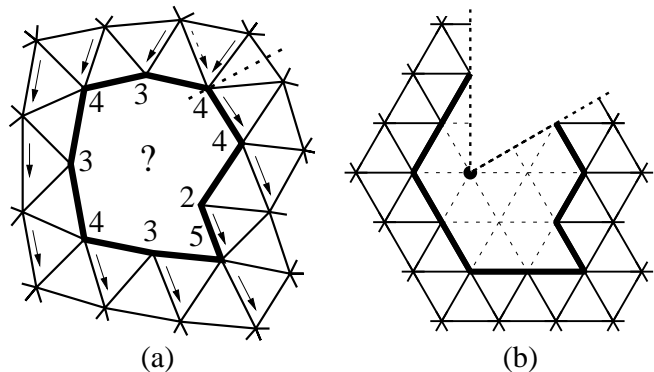


FIG. 13: A border with $W = 5$. Parallel transporting a direction around the border yields a rotation of 60° . A disclination must therefore be located within this border. The dashed line shows where we plan to cut. (b) We see the same border flattened onto a reference lattice. The 60° rotation is now more clear. The dashed lines are part of an equilateral triangle and therefore show the required location of a disclination. Any choice of cut results in the same location, as long as the of the cut is chosen so that the triangle is equilateral.

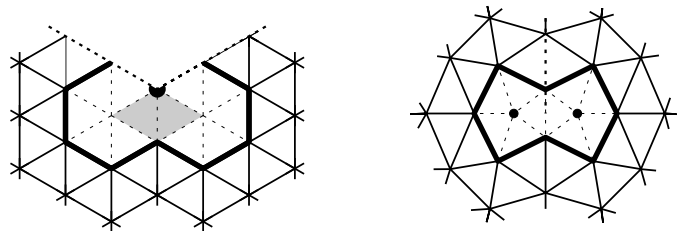


FIG. 14: Rearrangement of a $+2$ (120°) disclination located on a vertex into a pair of single disclinations with the same border. The two shaded triangles are removed.

two disclinations at the same point, we must move them slightly. FIGS. 14-15 show the two possible situations and equivalent fillings with only single disclinations and the same border. If the center is on a lattice point, then the disclinations can each move in opposite directions to neighboring points and the same region of the plane will be cut out, up to a triangle at the apex, as shown in FIG. 14. If the center is in the center of a triangle rather than on a lattice point, we can place the two disclinations on adjacent lattice points around the triangle for the same effect, as shown in FIG. 15. The disclinations can be further separated in a similar fashion.

This breaks down if the $+2$ disclination is on a vertex on the border which has 4 or more triangles. In this case there is no way to separate the disclinations without one of them crossing the border.

c. Three disclinations remaining

The case of $W = 3$ follows the same way, except now we find a $+3$ disclination on the midpoint of a line segment joining the two identified points. This $+3$ disclination

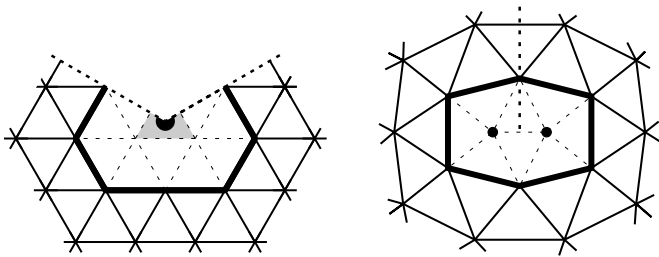


FIG. 15: Rearrangement of a +2 (120°) disclination located on a triangle into a pair of single disclinations with the same border. The shaded part of the triangle is removed.

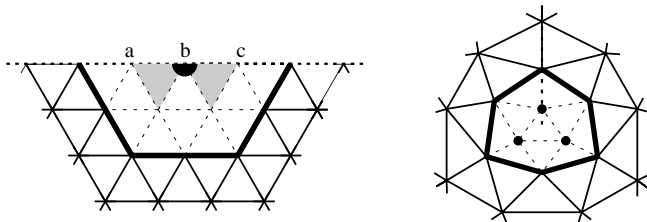


FIG. 16: Rearrangement of a +3 (180°) disclination located on a vertex into three single disclinations with the same border. The two shaded triangles are removed. Note that vertices a , b , and c all come together to form a single five-fold vertex.

may be on a lattice point or on the edge of a triangle. Both can again be split similarly to the previous case, as seen in FIGS. 16-17. As seen in the flattened pictures, the +3 disclination is always within the border, provided the flattened border does not intersect itself or the “cut line”. Thus outside of these cases, the border is only incompletable if the +3 disclination cannot be split properly without any single disclinations crossing a border.

APPENDIX B: STERIC CONSIDERATIONS

Our triangular units are two-dimensional objects but they represent three-dimensional structures in space. Thus, we must explicitly ensure that two triangles can

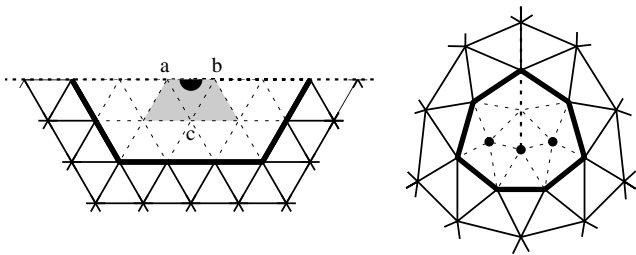


FIG. 17: Rearrangement of a +3 (180°) disclination located on an edge into three single disclinations with the same border. The three shaded triangles are removed and the vertices a , b , and c collapse to a single five-fold vertex.

never be in positions, such that the proteins they represent would overlap in space. This appendix collects details concerning the implementation of steric constraints. First (Sec. B 1) we write the explicit form of the term in our Hamiltonian that prevents self-intersection; then (Sec. B 2) we discuss the way in which steric constraints tend to assist growth and to discourage the wrong steps that lead to failure.

1. Steric potential

The final term in eq. (2.1) was a steric repulsion term: since our capsid units are two-dimensional triangles, some such term has to be added by hand, to account for the thickness of our three-dimensional proteins and disfavor unphysical configurations. The details of this term were deferred from Sec. II B to this appendix. The steric term should have the simplest possible form, in keeping with the toy-model spirit of our other terms.

In the steric term, the two kinds of degrees of freedom – topological and positional – clash in a sense. Two units that are nearby in space may be many steps apart on the bond network, and thus practically decoupled from each other. (There is little interaction in the elastic energy, and furthermore the ways they constrain the available discrete growth steps are independent.) Hence, $\mathcal{H}_{\text{steric}}$ must consist of topologically long-range, but positionally short-range, interactions.

We chose an implementation based on augmenting each triangle by another vertex over the face (on the interior side), thus forming a tetrahedron. We define a repulsion between the apex vertex of each tetrahedron and every (non-apex) vertex of every other triangle. Thus,

$$\mathcal{H}_{\text{steric}} = \sum_{I,j} V_{\text{steric}}(|\vec{r}_I^\Delta - \vec{r}_j|), \quad (\text{B1})$$

where \sum_I is a sum over triangles and \vec{r}_I^Δ is an equal distance $\ell_{\text{steric}} \lesssim r_0$ inward from the three vertices of the triangle. Furthermore, we require $V_{\text{steric}}(r) = 0$ if $r \geq \ell_{\text{steric}}$, which is the case for all pairs I, j in most capsids. This form allows the edges of unconnected triangles to be incident while maintaining $\mathcal{H}_{\text{steric}} = 0$ so long as the triangles do not actually intersect.

We choose the simplest form which is differentiable at $r = 0$ and $r = \ell_{\text{steric}}$,

$$V_{\text{steric}}(r) = k_{\text{steric}}(\ell_{\text{steric}}^2 - r^2)^2, \quad r < \ell_{\text{steric}}, \quad (\text{B2})$$

Choosing $\ell_{\text{steric}} \approx 0.65r_0$ generally provides sufficient stericity while not interfering with the shape of non-self-intersecting capsids.

It is important to stress that this steric term should not affect most capsids. For non-growing capsids, we generally turn it off to increase efficiency, since it always vanishes.

2. Steric growth heuristics

While the steric potential discussed in Sec. B1 is useful to prevent capsids from relaxing to unphysical positions, it does not directly help the growth rules. Because growth rules are based entirely on rates k_A , k_I , and k_J derived from the local geometry around individual vertices, there is no way to directly determine whether a step will cause a steric hindrance. Because such growth steps are not likely to occur in nature, we implement a heuristic to detect such steps and remove them from the set of allowed growth steps by setting the rate to zero.

Before any accretion or insertion, we perform two tests. First we look at the steric potential $\mathcal{H}_{\text{steric}}$. If the accretion causes $\mathcal{H}_{\text{steric}} \neq 0$ then the accretion fails. Next, if the accretion causes the centroid of one triangle to be within $\ell_{\text{steric}}/\sqrt{10}$ of the vertex of another triangle, then the accretion fails. This is necessary because the first test misses the case where two triangles are directly on top of one another. This case is less important while minimizing, because minimization would need to pass a large energy barrier, while growth steps can jump over it for free.

-
- [1] S. O. Kim, H. H. Solak, M. P. Stoykovich, N. J. Ferrier, J. J. De Pablo, and P. F. Nealey, *Nature* **424**, 411 (2003).
- [2] J. Y. Cheng, A. M. Mayes, and C. A. Ross, *Nature Mat.* **3**, 823 (2004).
- [3] D. H. Gracias, J. Tien, T. L. Breen, C. Hsu, and G. M. Whitesides, *Science* **289**, 1170 (2000).
- [4] G. M. Whitesides and B. Grzybowski, *Science* **295**, 2418 (2002).
- [5] D. J. Kushner, *Bacteriol. Rev.* **33**, 302 (1969).
- [6] R. N. Perham, *Phil. Trans. R. Soc. Lond. B. Biol. Sci.* **272**, 123 (1975).
- [7] M. F. Carlier, *Adv. Biophys.* **26**, 51 (1990).
- [8] F. U. Hartl and J. Martin, *Curr. Opin. Struct. Biol.* **5**, 92 (1995).
- [9] T. Ito, M. Bulger, M. J. Pazin, R. Kobayashi, and J. T. Kadonaga, *Cell* **90**, 145 (1997).
- [10] N. Kimizuka and T. Nakashima, *Langmuir* **17**, 6759 (2001).
- [11] J. N. Israelachvili, D. J. Mitchell, and B. W. Ninham, *Biochim. Biophys. Acta.* **470**, 185 (1977).
- [12] D. M. Salunke, D. L. D. Caspar, and R. L. Garcea, *Cell* **46**, 895 (1986).
- [13] R. F. Bruinsma, W. M. Gelbart, D. Reguera, J. Rudnick, and R. Zandi, *Phys. Rev. Lett.* **90** (2003).
- [14] V. S. Reddy, H. A. Giesling, R. T. Morton, A. Kumar, C. B. Post, C. L. Brooks, and J. E. Johnson, *Biophys. J.* **74**, 546 (1998).
- [15] It was noted early that capsids ought to be built from many identical copies of comparatively small proteins, in order to maximize the volume available for the genome, while minimizing the space on the genome needed to code them [48]. However, point group symmetries set an upper limit of 60 units which can be joined equivalently to form a closed convex polyhedron [16, 48]; thus many proteins must be inequivalent by the symmetry.
- [16] D. L. D. Caspar and A. Klug, *Cold Spring Harbor Symp. Quant. Biol.* **27**, 1 (1962).
- [17] L. Pauling, *Discussions of the Faraday Society* **13**, 170 (1953).
- [18] R. Zandi, D. Reguera, R. F. Bruinsma, W. M. Gelbart, and J. Rudnick, *Proc. Natl. Acad. Sci. USA* **101**, 15556 (2004).
- [19] B. Berger, P. W. Shor, L. T. Kellogg, and J. King, *Proc. Natl. Acad. Sci. USA* **91**, 7732 (1994).
- [20] R. Schwartz, P. W. Shor, P. E. Prevelige, and B. Berger, *Biophys. J.* **75**, 2626 (1998).
- [21] R. Schwartz, R. L. Garcia, and B. Berger, *Virology* **268**, 461 (2000).
- [22] A. Zlotnick, *J. Mol. Biol.* **241**, 59 (1994).
- [23] A. Zlotnick, *Journal of Molecular Recognition* **18**, 479 (2005).
- [24] J. A. G. Briggs, T. Wilk, R. Welker, H. G. Kräusslich, and S. D. Fuller, *EMBO J.* **22**, 1707 (2003).
- [25] B. K. Ganser, S. Li, V. Y. Klishko, J. T. Finch, and W. I. Sundquist, *Science* **283**, 80 (1999).
- [26] J. A. G. Briggs, K. Grünewald, B. Glass, F. Förster, H.-G. Kräusslich, and S. D. Fuller, unpublished work.
- [27] J. Benjamin, B. K. Ganser-Pornillos, W. F. Tivol, W. I. Sundquist, and G. J. Jensen, *Journal of Molecular Biology* **346**, 577 (2005).
- [28] B. K. Ganser-Pornillos, U. K. von Schwedler, K. M. Stray, C. Aiken, and W. I. Sundquist, *J. Virology* **78**, 2545 (2004).
- [29] L. S. Ehrlich, T. B. Liu, S. Scarlata, B. Chu, and C. A. Carter, *Biophys. J.* **81**, 586 (2001).
- [30] R. L. Kingston, N. H. Olson, and V. M. Vogt, *J. Struct. Biol.* **136**, 67 (2001).
- [31] M. Ge and K. Sattler, *Chemical Physics Letters* **220**, 192 (1994).
- [32] T. T. Nguyen, R. F. Bruinsma, and W. M. Gelbart, *Elasticity theory and shape transitions of viral shells* (2005), physics/0506127.
- [33] J. Lidmar, L. Mirny, and D. R. Nelson, *Phys. Rev. E* **68** (2003).
- [34] D. Endres, M. Miyahara, P. Moisant, and A. Zlotnick, *Protein Sci* **14**, 1518 (2005).
- [35] A. Zlotnick, R. Aldrich, J. M. Johnson, P. Ceres, and M. J. Young, *Virology* **277**, 450 (2000).
- [36] J. A. Speir, S. Munshi, G. Wang, T. S. Baker, and J. E. Johnson, *Structure* **3**, 63 (1995).
- [37] P. Forrer, C. Chang, D. Ott, A. Wlodawer, and A. Pluckthun, *Journal of Molecular Biology* **344**, 179 (2004).
- [38] Z. Xie and R. W. Hendrix, *Journal of Molecular Biology* **253**, 74 (1995).
- [39] D. C. Rapaport, *Phys. Rev. E* **70** (2004).
- [40] D. Endres and A. Zlotnick, *Biophys. J.* **83**, 1217 (2002).
- [41] A. Zlotnick, *Virology* **315**, 269 (2003).
- [42] H. S. Seung and D. R. Nelson, *Phys. Rev. A* **38**, 1005 (1988).
- [43] These are both consequences of the Euler characteristic for a genus 0 surface, $\chi(g) = 2 - 2g = 2$. More generally, $V - E + F = \chi(g)$, and the total

disclination charge must sum to $2\pi\chi(g)$. For more information, see Eric W. Weisstein. “Euler Characteristic.” From MathWorld—A Wolfram Web Resource. <http://mathworld.wolfram.com/EulerCharacteristic.html> and references therein.

- [44] I. L. Ivanovska, P. J. de Pablo, B. Ibarra, G. Sgalari, F. C. Mackintosh, J. L. Carrascosa, C. F. Schmidt, and G. J. Wuite, *Proc Natl Acad Sci U S A* **101**, 7600 (2004).
- [45] For a discussion of the geometric considerations in phage head assembly, see M. F. Moody, *J Mol Biol* **293**, 401 (1999).
- [46] A 7-fold vertex has a negative disclination charge; there

must be a 5-fold vertex next to it, with its positive disclination charge so the interior of the loop is neutral. A pair or “dipole” of positive and negative disclinations constitutes a *dislocation*. Its presence could have been concluded by the non-zero Burgers vector associated with that same loop; that is, the sum of the lattice displacements of each step, referenced to the ideal triangular lattice that can exist far away from this hole.

- [47] ℓ_f can be made dimensionless by dividing by r_0 .
- [48] F. H. C. Crick and J. D. Watson, *Nature* **177**, 473 (1956).